Outer target heat fluxes and power decay length scaling in L-mode plasmas at JET and AUG

A. Scarabosio[1], T. Eich[1], A. Herrmann[1], B.Sieglin[1],

the ASDEX Upgrade Team[1] and JET-EFDA contributors*

JET-EFDA, Culham Science Centre, Abingdon, OX14 3DB UK,

[1] *Max-Planck-Institut für Plasmaphysik, EURATOM Association, Boltzmannstr 2., D-85748 Garching, Germany.*

* *See the Appendix of F. Romanelli et al., Proceedings of the 23rd IAEA Fusion Energy Conference 2010, Daejeon, Korea.*

Abstract

Experimental measurements of heat load profiles from infrared thermography in L-mode plasmas from two tokamaks, JET and ASDEX Upgrade, are presented. The power decay length (λ_q) is extracted via a fitting procedure. The basic dependencies of λ_q are identified through plasma parameters scans and for the case of fully attached divertor using numerical regressions (after mapping at the mid-plane). The results are compared with previously published H-mode data. Qualitatively, similar trends with the safety factor, toroidal magnetic field and heating power are found though bulk data is about a factor of two larger in L-mode for both devices. Consistently a clear shrinking of the heat channel width is observed at the L-H transition linked with the formation of the pedestal temperature. Extrapolation of the empirical power scaling laws to ITER gives $\lambda_q \simeq$3.0-4.9mm for L-mode plasma.

Key words: JET, ASDEX-Upgrade, Edge plasma, Divertor

PACS: 52.55.Tn, 52.55.Fa, 52.55.Rk

1 Introduction

Although power dissipation in the divertor will ultimately determine the target peak heat load (q_{max}), the power decay length in the SOL above the X-point region λ_q, is a crucial quantity governing exhaust dynamic in tokamaks. For instance, achievement of detachment is expected to depend strongly on λ_q. Also, during the discharge evolution (L-to-H, H-to-L, instabilities etc...), enough power dissipation may not be reached at all times resulting in a power deposition directly linked to λ_q. Despite the importance of an accurate prediction of λ_q, a commonly accepted theoretical model or empirical extrapolations from current devices to ITER remain elusive [1]. In recent work [2], outer target heat flux profiles from the JET and ASDEX Upgrade tokamak have been used to derive the inter-ELM λ_q H-mode [2] with fully attached divertor. Low recycling attached divertor represents the best possible condition to infer λ_q from target data when others, more direct measurements, are not available. In this case it is found that the target heat flux profile from thermography can be represented as the convolution of an exponential function with decay λ_q and a gaussian of width S, as due to a residual radial diffusion in the divertor. The results were used to extract a scaling law for λ_q (magnetically mapped at mid-plane dividing by the flux expansion f_x) with plasma parameters and

* Max-Planck-Institut für Plasmaphysik, EURATOM-Association, Boltzmannstr. 2, D-85748, Garching, Germany

successfully compared with an heuristic model [3]. These results have been confirmed by similar analysis in DIII-D and C-Mod [4]. To further test and complete the physical understanding the effect of ELMs, plasma density and confinement must also be clarified. In this work we apply the same methodology as in [2] to L-mode plasmas from the JET and ASDEX Upgrade tokamaks. Since it is desirable to achieve the L-H transition at relatively low plasma density, due to the lower power threshold, $\lambda_{q,L-mode}$ may also have direct impact on the H-mode accessibility and operation of large devices such as ITER.

2 The L-mode database and the analysis

We consider only discharges with carbon divertor plasma-facing components. The present database includes, respectively, 19 hydrogen and 21 deuterium JET plasmas, and 29 deuterium AUG plasmas. L-mode helium plasma are available for both machines and will be included in the database in the future. Important parameters are summarised in Table 1. We denote plasma current as I_p,toroidal magnetic field as B_T, edge safety factor as q_{95}, heating power as P_h, triangularity as δ, and the plasma density as n_p. The aspect ratio of both machines, defined as $\epsilon = a/R_{geo}$, is ϵ=0.32, with the major geometrical radius denoted as R_{geo} and the minor radius as a. The plasma elongation amounts to κ=1.6 for both devices. Different divertor plasma conditions are included, ranging from fully attached low recycling with peak target temperature of around 30eV to partially detached with target temperature of a few eV. The JET database contains limited q_{95} and P_h scans in hydrogen and density scans in deuterium. The AUG database is relatively old (discharges performed between 2002-2006) and sparse with no dedicated experiments.

2.1 Characterisation of heat flux profile and the extraction of the decay length

The SOL power decay length is determined by analysis of heat flux profiles measured at the outer divertor target by means of infrared thermography. Details of the experimental setup for JET can be found in [5] and for AUG in [6].

Following [2] and expressing the target coordinate as s and the strike line position on target as s_0 we describe the heat load profile at the divertor entrance as

$$q(\bar{s}) = q_0 \cdot \exp\left(-\frac{\bar{s}}{\lambda_q}\right) \text{ and } \bar{s} = s - s_0 \ , \ s \geq s_0 \tag{1}$$

This simple ansatz allows for the accounting of the perpendicular heat diffusion or *leakage* into the private-flux-region (PFR) by introducing a Gaussian width S representing the competition between parallel and perpendicular heat transport in the divertor volume. This means that, physically, the exponential profile at the divertor entrance [7], is diffused into the private flux region while travelling towards the target [8]. This competition is approximated by a convolution of the exponential profile with a gaussian function with the width S. Neglecting the flux expansion f_x the target heat flux profiles are thus expressed as ($s \in [-\infty, \infty]$)

$$q(\bar{s}) = \frac{q_0}{2} \exp\left(\left(\frac{S}{2\lambda_q}\right)^2 - \frac{\bar{s}}{\lambda_q}\right) \cdot \operatorname{erfc}\left(\frac{S}{2\lambda_q} - \frac{\bar{s}}{S}\right) + q_{BG} \tag{2}$$

Figure 1 shows two examples, one for JET and one for AUG, of the measured heat flux profiles and fitting results by using Eq.2 with the free parameters $S, \lambda_q, q_0, q_{BG}$ and s_0. In the figure we also depict the extrapolated exponential heat flux profile from Eq.1. Note that this procedure allows an independent

estimation of the strike point position at the target. From Eq.2 follows the integral power decay width [9]

$$\lambda_{int} = \frac{\int (q(s) - q_{BG}) ds}{q_{max}} \tag{3}$$

This quantity is frequently used in the literature [9] since it allows to relate the peak heat load on the divertor target to power deposited on the divertor target, a crucial design parameter for the power handling capabilities of a large device such as ITER. Within the framework model of Eq.2 the relation between exponential and integral decay lengths can be written with good approximation as (also neglecting q_{BG}) [4]

$$\lambda_{int,model} \simeq \lambda_q + 1.64S \tag{4}$$

As figure of merit for the fit quality we plot in figure 2, and for the entire database, the ratio $\lambda_{int}/\lambda_{int,model}$ with λ_{int} calculated from the experimental profiles using Eq.3. It can be seen that this ratio is always close to one indicating satisfactory fit. Small systematic deviation (ex. for the AUG data) can be mainly ascribed to the residual background in the heat flux profile. It is quite surprising that this simple model equation fits well heat flux profiles also in presence of partial power detachment where complex physical processes are already taking place in the divertor volume. This complex physics can apparently be captured by the effective radial diffusion parameterised by the gaussian width S.

More importantly, it should be noted that any physical study of the SOL power decay length should use λ_q and not λ_{int} which has a stronger dependence on the divertor physics as seen from Eq.2. For instance attempts to regress the data would lead to different results if using λ_q or λ_{int}.

3 λ_q dependence on basic plasma parameters

Basic main plasma dependencies are best studied using systematic parameter scans (while fixing all others as much as possible) in a single or subsequent discharges. Within the present database we have available very limited q_{95} scan (at fixed I_p) at two different P_h in JET hydrogen plasmas and density steps in JET deuterium plasmas. Despite this limitation, figure 3 shows a clear monotonic increase of λ_q with q_{95} for both P_h values. Also, λ_q is larger for higher heating power at the same safety factor. Note that these scans are performed at fixed I_p thus $q_{95} \propto B_t$. The observed behaviour can be equally attributed to the toroidal field. No q_{95} scan at fixed B_t are available. To disentangle these dependencies a parametric regression of the decay length is shown in the next section which confirms the role of the safety factor.

In the following we concentrate on fully attached (generally low density) plasmas leaving the discussion of n_p effect for future publication. We only anticipate that, for fixed input power, a moderate plasma density variation has a weak effect on λ_q while it is more evident on the diffusion parameter S which tends to increase leading to a more 'Gaussian shaped' profile (with much smaller q_{max}).

4 Scaling of λ_q in AUG and JET L-mode plasmas

We apply least square fitting to derive a parametric dependency of the power decay length. To make the data from both devices more homogeneous and to allow better extrapolation of the SOL properties of λ_q we: i) select plasmas with fully attached target condition having low upstream density (JET crite-

rion) and peak target electron temperature above 8eV (AUG criterion). ii) We select fits with $S/\lambda_q < 0.60$. This is because two-dimensional numerical heat diffusion calculations [10] using Spitzer parallel and Bohm perpendicular thermal diffusivities show that using Eq.2 is accurate to better than 5% in determining λ_q at the divertor entrance in cases where the deduced Gaussian width S is less than 60% of the exponential width λ_q. After data selection we have 15 hydrogen and 7 deuterium JET plasmas and 13 deuterium AUG plasmas. iii) In order to relate the surface heat flux profile to the outer midplane separatrix region, the magnetic flux expansion, f_x, has to be taken into account. We use the definition for an integral flux expansion along the target surface[6,9] calculated for the outer midplane region $R = R_{sep}$ to $R = R_{sep} + 5\,\mathrm{mm}$, with R_{sep} being the outer separatrix radius. Thus we define and regress the quantity $\lambda_q \equiv \lambda_q / f_x$ using the following variables: toroidal field B_T, cylindrical safety factor q_{cyl} (for JET only) or edge safety factor q_{95} (for AUG and combined data from both devices), power crossing the separatrix P_{SOL} and R_{geo} when regressing combined data. We assume the following functional dependency:

$$\lambda(\mathrm{mm}) = C_0 \cdot B_T^{C_B}(\mathrm{T}) \cdot q^{C_q} \cdot P_{SOL}^{C_P}(\mathrm{MW}) \cdot R^{C_R}(\mathrm{m}) \tag{5}$$

The selected data showed no statistically significant dependence on the plasma density and it is thus excluded from the fit parameters (despite a non negligible variation $n_p = 1.9 - 4.2 \cdot 10^{19} m^{-3}$). The summary table 2 shows the data used for each regression, the exponent and error bars for each variable and the quality of the fit (degrees of freedom adjusted correlation coefficient R^2). The quality of the fit changes considerably from case to case and the error bar on parameters can be large. Nevertheless and quite remarkably, we find the same qualitative dependencies for all combinations of data used. Namely a nearly linear increase of λ_q with the safety factor which is always the parameter with

the largest exponent. In general, no satisfactory fit can be obtained without using this variable. A still positive but much weaker dependence on P_{SOL} and a negative B_t with an exponent in the range $[-0.8, -0.4]$ for the combined database. The highest correlations are found by using hydrogen JET data only and hydrogen JET plus AUG data (80% of the database). This latter case is also plotted in figure 4. In this case the scaling law reads as:

$$\lambda_q = 1.44 \pm 0.67 \cdot B_T^{-0.80\pm0.32} \cdot q_{95}^{1.14\pm0.67} \cdot P_{SOL}^{0.22\pm0.10} \cdot R^{-0.03\pm0.28} \tag{6}$$

Two important results must be pointed out. First, the L-mode scaling in Eq.6 (as well as the one of JET hydrogen only) is very similar to the JET H-mode scaling (see table 2 in [2]) with the exception of the double proportional coefficient, suggesting a tendency for larger λ_q in L-mode. Second, the major R dependence is basically negligible, again similar to the previous finding in H-mode. The regression of the entire database, including JET deuterium, is shown in figure 5. The most important difference is the appearance of a major R dependency. We believe this is mainly an artifact. The inclusion of R in the regression in fact does not improve substantially the fit quality (see last row of table 2) and the associated uncertainty is larger than the exponent itself. This large uncertainty is due to the large cross-correlation with P_{SOL} within this database (large P_{L-H} threshold for larger machine). These results are different from the L-mode scaling law developed by A. Loarte et al. in [9], especially regarding the major R and q_{95} dependency. Our L-mode scaling is closer, in terms of main dependencies, to the H-mode scaling proposed also in [9]. One reason is that here we concentrated on the attached L-mode cases only where divertor effects are, in principle, minimised.

5 Comparison with H-mode plasmas

The results of the previous section suggest the need of a more detailed comparison between L-mode and H-mode data. Figure 6 show a comparison of $\lambda_{q,L-mode}$ with the H-mode scaling law $\lambda_{q,H-mode} = 0.73 \cdot B_t^{-0.78} q_{cyl}^{1.20} P_{SOL}^{0.10} R^{0.02}$. We can see that for most cases $\lambda_{q,L-mode}$ is $2-3$ times larger than predicted by the scaling law. This is expected since radial transport in L-mode is larger than in H-mode in the main plasma, SOL and apparently also in the divertor as suggested by larger diffusion parameter S (not shown). This feature becomes more evident when looking at the heat flux profiles during an L-H transition as illustrated in figure 7 for a JET deuterium plasma. The NBI power step-up initiates a fast temperature increase. After about 100ms a dithering phase visible in the integrated power to the target and H_α signal (not shown) coincides with a sudden shrinking of the heat flux channel with a reduction of λ_q by almost a factor of 2. After another 200ms λ_q has reached its ELM-free H-mode value which is in line with inter-ELM scaling (see figure 6). Also S decreases by about 30% in the ELM-free H-mode regime. Analysis of the kinetic profiles shows that the shrinking of the heat flux channel is linked with the changes in the pedestal temperature (pedestal density evolves much more slowly). The rapid change in λ_q around t=63.65s happens in few tens of ms, much shorter time than the energy confinement time. Stationary heat flux profile is reached when $T_{epedestal}$ has reached about 90% of its final value.

This observation may have important consequences for the operation of large device such as ITER reducing the H-mode accessibility. In fact, the ELM-free period before the first ELM (lasting in this case more than 0.5s) will be a very critical one in terms of heat loads. Not only the exhaust channel has became

very narrow (perhaps even narrower than the H-mode scaling in [2] predicts), but during this period the broadening affect associated with the strike point movement during ELM cycle [2] is also absent as only a 5-6mm slow drift of the peak heat flux is observed.

6 Summary and discussion

We have constructed and analysed a database of heat flux profiles for JET and AUG L-mode plasmas. The fitting procedure successfully applied to H-mode plasmas works well also for L-mode, both with attached and partially power detached divertor. Despite certain quantitative variation, we find, for fully attached cases, positive trend of λ_q with the safety factor ($\sim q_{95}^{0.73\div1.14}$) and input power ($\sim P_{SOL}^{0.13\div0.29}$) and negative dependence with the toroidal field ($\sim B_t^{-0.80\div-0.40}$). Within the present database a weak dependence on machine size cannot be yet excluded but it seems, however, unlikely. If confirmed, this similarity with the H-mode scaling calls for theoretical understanding lacking at present. We find no clear difference between hydrogen and deuterium plasmas. The numerical coefficients of the empirical power scaling law found here in L-mode and the one in H-mode [2] are in agreement within error bars except a proportionality factor about two times larger for L-mode. This same result is found when looking at λ_q during the L-H transition which shows a sudden reduction linked with the pedestal temperature change. The L-H transition will be a very critical phase for the exhaust control during ITER operation. We finally extrapolate these results to the λ_q in ITER L-mode (see last column of table 2) using the design value R=6.2 m, a=2.0 m, κ=1.7, B_{tor}=5.3 T, I_p=15 MA, q_{95}=3.0 and a maximum L-mode SOL power

P_{SOL}=50 MW before transition to H-mode. We find λ_{SOL} $\simeq$3.0-4.9mm, which, although smaller than currently predicted, should pose no serious problem to the machine operation.

7 Acknowledgement

This work was supported by by EURATOM and carried out within the framework of the European Fusion Development Agreement. The views and opinions expressed herein do not necessarily reflect those of the European Commission.

References

[1] A. Loarte et al., Nucl. Fusion 47 (2007) S203S263.

[2] T. Eich et al., Phys. Rev. Lett. 107 (2011),215001.

[3] R.J. Goldston, Nucl. Fusion 52 (2012) 013009.

[4] M. A. Makowski, accepted for publication in Physics of Plasmas.

[5] T. Eich et al., J. Nucl. Mater. 415, S856 (2011).

[6] A. Herrmann et al., Plasma Phys. Controlled Fusion 44, 883 (2002).

[7] P. Stangeby et al., Nucl. Fusion 50, 125003 (2010).

[8] A. Loarte et al., Contrib. Plasma Phys. 32, 468 (1992).

[9] A. Loarte et al., J. Nucl. Mater. 266269, 587 (1999).

[10] R.J. Goldston, Phys. Plasmas 17, 012503 (2010).

8 Figure captions

Fig. 1. Example of heat flux profiles measured on the outer divertor target and fits using Eq. (2). The red solid tick line is the extracted exponential heat flux profile at the divertor entrance.

Fig. 2. Comparison of λ_{int} calculated from experimental profile (Eq.3) and λ_{int} from the model equation Eq.2 using fit parameters λ_q and S. Values near unity indicate fit good quality.

Fig. 3. Safety factor and heating power effects on λ_q in three consecutive hydrogen JET discharges.

Fig. 4. Scaling law for JET hydrogen and AUG deuterium data. Red star symbols are JET blue squares are AUG.

Fig. 5. Scaling law for combined JET (hydrogen and deuterium) and AUG data. Red star symbols are JET blue squares are AUG.

Fig. 6. Comparison of L-mode data with H-mode scaling in [2]. Only fully attached L-mode plasmas are plotted.

Fig. 7. Decay length λ_q and S evolution during the L-H transition at JET.

9 Table captions

Table 1

Database of the analysed discharges.

Table 2

Parameter dependency of $\lambda_q = \lambda_q / f_x$ for various combinations of JET and AUG data.

10 Figures

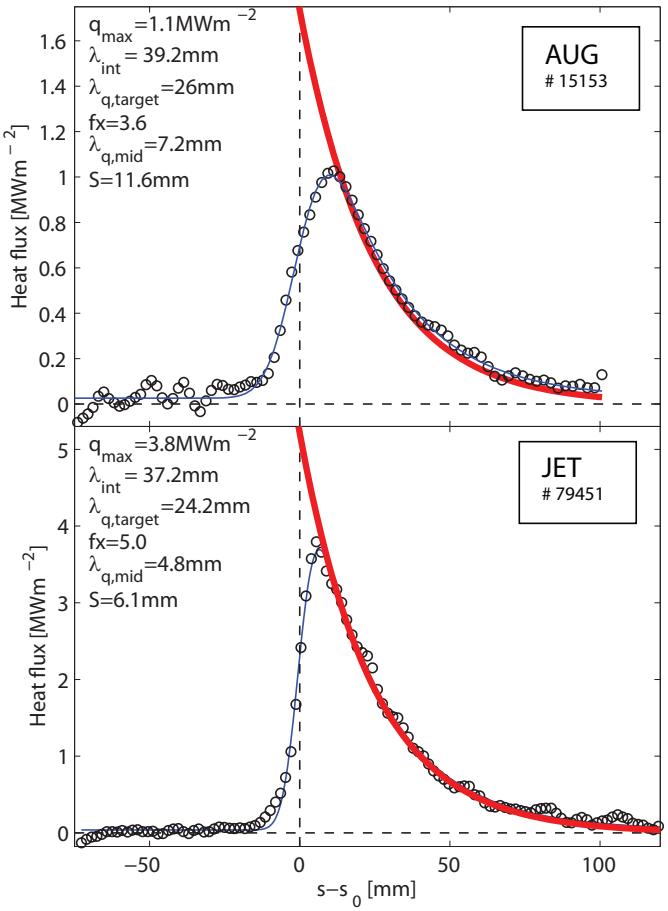

Figure 1

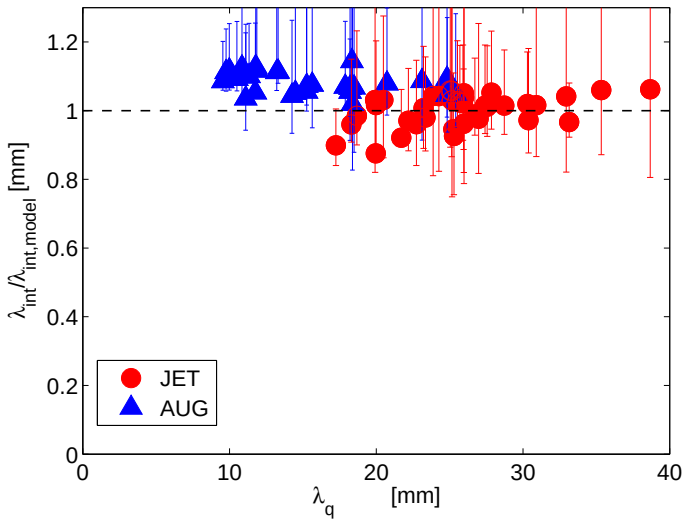

Figure 2

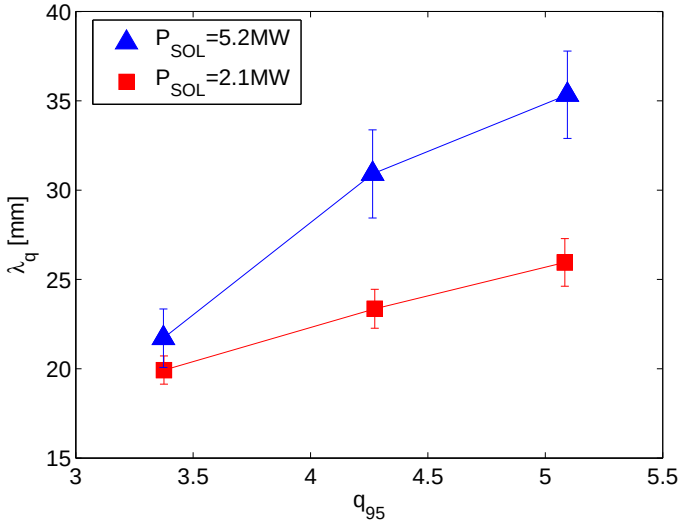

Figure 3

11 Tables

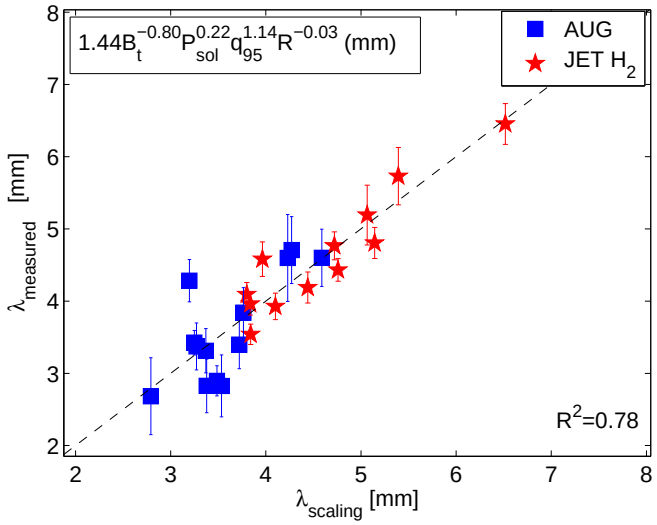

Figure 4

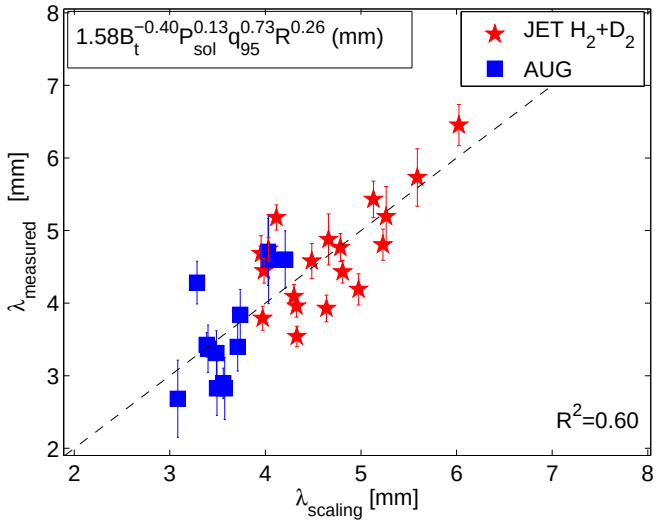

Figure 5

Table 1

	Gas	I_p [MA]	B_t [T]	q_{95}	P_h [MW]	δ	n_p [10^{19}m^{-3}]
JET	H_2	1.5-2.5	1.5-3.1	3.3-5.1	1.7-6.0	0.16-0.41	2.0-3.8
JET	D_2	1.5-3.0	1.5-2.7	2.9-5.6	1.5-5.5	0.15-0.41	1.9-4.2
AUG	D_2	0.6-1.0	1.8-2.7	3.4-5.8	0.4-2.3	0.06-0.12	1.9-4.2

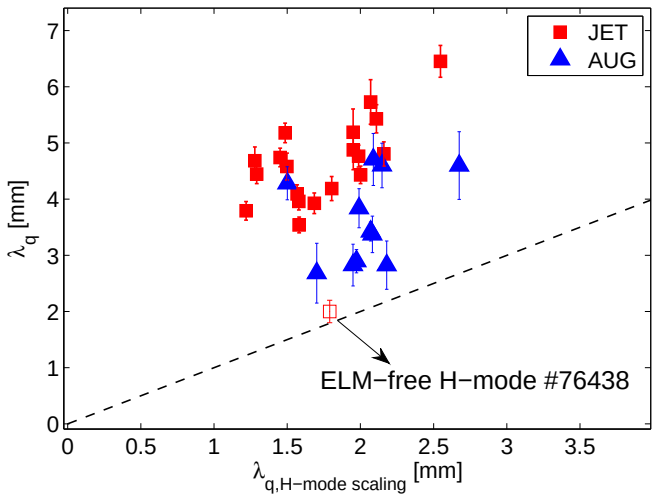

Figure 6

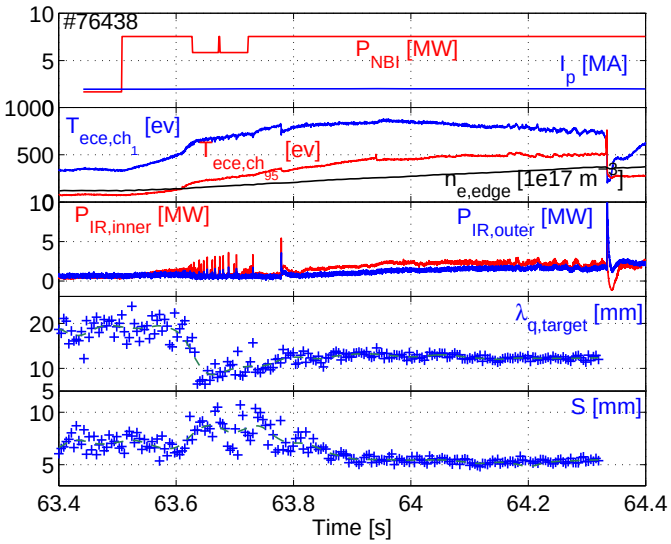

Figure 7

Table 2

JET	AUG	C_0	C_B	C_q	C_P	C_R	R^2	$\lambda_{ITER}[mm]$
H_2	-	1.86±0.45	-0.66±0.19	0.93±0.25	0.29±0.07	-	0.93	4.4
H_2, D_2	-	2.40±0.98	-0.37±0.30	0.68±0.37	0.18±0.13	-	0.49	4.6
	D_2	4.37±2.64	-2.41±1.04	1.32±0.49	0.27±0.17	-	0.79	-
H_2	D_2	1.44±0.67	-0.80±0.33	1.14±0.67	0.22±0.10	-0.03±0.28	0.78	3.0
H_2, D_2	D_2	1.58±0.83	-0.40±0.31	0.73±0.32	0.13±0.11	0.26±0.30	0.60	4.9
H_2, D_2	D_2	2.06±0.90	-0.54±0.29	0.76±0.33	0.21±0.07	-	0.57	-